Ecological Modelling 313 (2015) 149–161

Contents lists available at ScienceDirect

Ecological Modelling

journal homepage: www.elsevier.com/locate/ecolmodel

Modelling the effect of wave forces on subtidal macroalgae: A spatial evaluation of predicted disturbance for two habitat-forming species

Timothy Jones*, Jonathan P.A. Gardner, James J. Bell

School of Biological Sciences, Victoria University of Wellington, PO Box 600, Wellington 6140, New Zealand

ARTICLE INFO

Article history:
Received 14 April 2015
Received in revised form 18 June 2015
Accepted 19 June 2015

Keywords:
Marine biomechanics
SWAN wave model
Macrocystis pyrifera
Ecklonia radiata
Kelp forests
Wave disturbance

ABSTRACT

In shallow marine environments, wave-induced disturbance can have a major influence on species abundance and distribution patterns. Understanding how waves affect habitat engineers, such as macroalgae, is therefore important for understanding subtidal community dynamics. In this study a wave model (SWAN) was used to identify the spatial distribution of wave forces across the Wellington south coast (New Zealand) for average and extreme conditions. The predicted distribution of wave-induced disturbance for two macroalgal species was then evaluated by applying wave-model predictions to a biomechanical threshold for *Ecklonia radiata* and to parameterise a biomechanical model that predicts probability of stipe failure for giant kelp, *Macrocystis pyrifera*. Analyses revealed that direct damage to *E. radiata* was unlikely as a result of regular wave conditions consistent with it being widespread in this region. However, storm conditions could cause damage to *E. radiata* plants across ~40% of rocky reefs where *E. radiata* occurs, but would likely only affect the largest individuals, potentially imposing a spatially variable upper size limit in *E. radiata* communities. Across all locations stipe failure probabilities for *M. pyrifera* were predicted to be <15% during storm events and <5% under frequently occurring wave conditions. However, there was a negative correlation between the presence of *M. pyrifera* and predicted stipe failure probabilities, suggestive of wave-induced limitation despite the low predicted failure rates. This study represents a novel application of wave modelling to understand how biomechanical thresholds act on a geographic level, and provides an important step-forward in advancing a mechanistic understanding of macroalgal distributions.

1. Introduction

Studying the physical factors experienced by species has played a key role in the field of ecology. An important area of research has been the identification of species-specific thresholds and tolerances to these physical factors (Kearney and Porter, 2009) and how they influence species distribution patterns (Elith and Leathwick, 2009). In shallow marine environments, wave related forces comprise some of the most important physical forces governing the abundance and distribution of species (England et al., 2008; Hill et al., 2010; Burrows, 2012). The most prominent effect of wave forces is the biomechanical effect it imposes on individuals, with subsequent effects on the rate or the probability of damage and mortality (Gaylord et al., 1994; Denny and Gaylord, 2002, 2010). Wave forces have been shown to induce an upper limit on the size of macroalgal species (Gaylord et al., 1994; Blanchette, 1997), as well as controlling the size and shape of hard coral colonies across a coral reef (Madin and Connolly, 2006), while wave-related indices, such as fetch, have been related to subtidal (Hill et al., 2010; Burrows, 2012) and intertidal community composition (Burrows et al., 2008). However, wave exposure has been shown to also benefit some species of macroalgae due to increased nutrient uptake and photosynthetic efficiency by constant rearrangement of algal fronds (Leigh et al., 1987; Duggins et al., 2003).

The major influence of wave action on marine species means that knowledge of the wave forces experienced at different locations is vital in order to understand and explain differences in marine community structure and dynamics among locations (Hill et al., 2010). While there is no replacement for measuring wave-exposure directly, either using dynamometers (Carrington-Bell and Denny, 1994), or direct wave height using electronic loggers such as wave rider buoys (Wright, 1976), these methods are often expensive to maintain (electronic loggers), or logistically unsuitable (dynamometers need to be deployed in great numbers) for obtaining metrics of wave exposure over large enough areas to enable large-scale evaluations (1–10's km). An alternative to

* Corresponding author.
E-mail address: timothy.t.jones@gmail.com (T. Jones).

http://dx.doi.org/10.1016/j.ecolmodel.2015.06.026
0304-3800/

these approaches consists of constructing models based on wave physics to predict wave exposure. SWAN (Simulating WAves Nearshore—http://swanmodel.sourceforge.net/) is a third generation numerical wave model that models wave generation and dissipation through their interaction with local wind patterns and the seabed as they propagate into coastal shelf areas (Booij et al., 1999; Ris et al., 1999). SWAN can be applied at any scale relevant to coastal applications, and includes terms that model wind-generation, depth-induced wave breaking and wave-wave interactions that can enhance or dissipate wave energy (Booij et al., 1999; Ris et al., 1999). SWAN models have previously been applied in oceanographic (Ris et al., 1999) and coastal engineering scenarios (Warner et al., 2008), but have not been used extensively in marine ecology (however, see England et al., 2008; Huang et al., 2012).

The aim of this study was to develop a SWAN wave model to identify the variation in wave forces and the extent to which macroalgal communities may be influenced by waves along the Wellington south coast in New Zealand. The Wellington south coast frequently experiences swell with an average significant wave height of 2.25 m as well as seasonal storms that can give rise to extended periods where wave heights can reach up to 5–8 m in height (Pickrill and Mitchell, 1979; Carter and Lewis, 1995). In addition, the Wellington south coast is characterised by macroalgal assemblages (Choat and Schiel, 1982; Pande and Gardner, 2009) that are particularly speciose (Nelson, 2008). Using the wave model, the magnitude and distribution of wave forces are examined for waves that occur regularly along the Wellington south coast, as well as for extreme conditions that occur on an annual basis as a result of winter storms. This information is then applied to predict the spatial distribution of disturbance in macroalgal communities through biomechanical assessments of how waves affect two species of subtidal macroalgae that are present along Wellington's south coast; *Macrocystis pyrifera* and *Ecklonia radiata*. These species differ both in terms of their morphology, with *E. radiata* reaching a maximum length of 2 m (Wernberg et al., 2003), whereas *M. pyrifera* can attain lengths greater than 25 m (Stewart et al., 2009), and also their distribution along the Wellington south coast, with *E. radiata* being widespread and abundant (Choat and Schiel, 1982; Pande and Gardner, 2009), whereas *M. pyrifera* has a much patchier distribution (Hay, 1990). However, both species form dense canopies, modifying the physical environment and providing biogenic habitats for many species of fish and invertebrates (Clark et al., 2004; England et al., 2008). Elucidating the wave forces in relation to their mechanical thresholds can therefore yield information regarding the probabilities and frequencies of disturbance within these habitats, as well as setting limits for species-specific distribution, size and abundance and how these relate to differences in community composition among locations. The results of the wave model and subsequent biomechanical analyses are also related to the distributions of these species in order to better understand whether the distributions are related to the probability of wave-induced disturbance.

2. Methods

The SWAN wave model simulates wave propagation and calculates how wave parameters evolve due to interactions with the seafloor and local wind patterns (Booij et al., 1999; Ris et al., 1999). The model requires spatially explicit bathymetry data, boundary wave conditions and local wind strength and direction. The methods are split into sections describing data acquisition required for the wave model, wave model operation and its outputs and the application of model predictions to the biomechanics of *E. radiata* and *M. pyrifera*. For more details, as well as limitations of the SWAN model, see Supplementary material.

2.1. SWAN model area—Bathymetry and substrate information

The study area was defined as the nearshore area from Breaker Bay (41°19.8′S, 174°50.4′E) to Sinclair Head (41°21.48′ S, 174°42.36′E) because model results for this area are likely to be most useful with regard to matching wave forces to biological community composition based on previous (Pande and Gardner, 2009) and ongoing studies (Fig. 1). The wider computational domain had to be large enough so that edge effects (arising from the undefined eastern and western ocean boundaries—see Supplementary material) were unlikely to affect model predictions for the area of interest. In addition, wave action in this area is likely to be affected by the headland east of the Wellington Harbour entrance, so this was also incorporated into the computational domain resulting in a 27,270 m (east-west) by 13,050 m (north-south) grid (Fig. 1).

Bathymetry and substrate data (substrate data were used to examine model results on areas of different substrates) for this area were obtained from the National Institute of Water and Atmospheric Research (NIWA) in New Zealand. These data were collected at 2 m resolution by multibeam soundings using NIWA's deepwater research vessel *Tangaroa*. Due to the constraints of ship-based bathymetry acquisition there were gaps in the data for some nearshore areas. Depths and substrate types for those gaps in the data were predicted using aerial imagery and interpolation based on bathymetry and nautical charts (see Supplementary material). The resultant bathymetry and substrate datasets consisted of 2 m resolution gridded maps for the entire computational domain (see Supplementary material).

2.2. SWAN model conditions—Wind and wave regimes

Wellington's south coast experiences waves often as a result of weather systems in the Southern Ocean (Carter and Heath, 1975; Carter and Lewis, 1995) and are therefore not generated inside of the model area. These waves were modelled by specifying incoming wave conditions (significant wave height, period and direction) along the southern computational boundary based on hindcast wave predictions from a global wave model. Data from NOAA wavewatch III (Tolman, 1997) were obtained for the nearest virtual buoy location (41°30′S, 174°30′E) for the period February 2005 to May 2011. The data consisted of hindcast predictions of wave period, direction and significant wave height at three hourly intervals. Local wind speed and direction data was obtained from the NIWA national climate database (NIWA, 2012) for the Wellington Airport station (41°19.32′S, 174°48.24′E) over the same time period. To identify separate wave regimes the wind/wave data were aligned (i.e. time matched) and split into separate classes based on (i) wind speed, (ii) wind direction, (iii) wave height and (iv) wave direction (see Supplementary material for data on all wave scenarios). The separate values for each wind/wave parameter were averaged across all records within each class, with the resulting wave parameters used to define boundary wave conditions whilst wind parameters were used to define a uniform wind field. We specifically focus on two wind/wave scenarios that are representative of regular and extreme conditions. Wave class 18 (Table 1) was the most frequent wave class identified, with corresponding conditions occurring on ~20 days per year and is representative of regularly occurring southerly swell conditions (henceforth referred to as regular wave conditions). Wave class 21 (Table 1) was the most extreme class identified (i.e. largest wave height and wind speeds) with conditions occurring for approximately one day per year and is therefore representative of storm conditions that may occur on an annual, or biennial basis (henceforth referred to as storm conditions). By examining these wind/wave scenarios we can evaluate predicted disturbance for *E. radiata* and *M. pyrifera* under regular

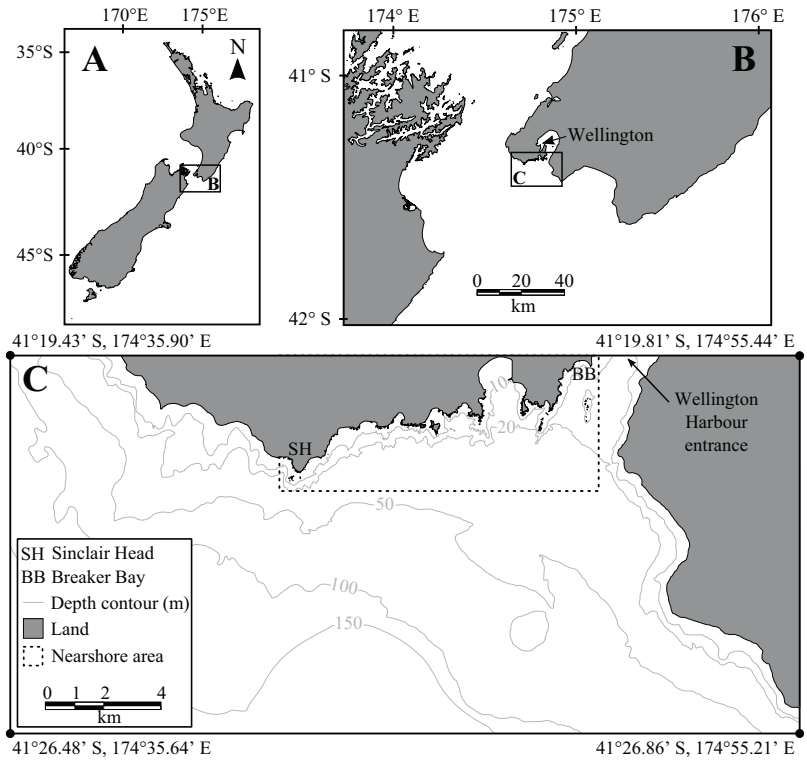

Fig. 1. Maps showing (A) New Zealand with insets showing (B) the southern tip of the North Island and (C) the location and extent of the computational grid with contour lines illustrating bathymetry along with the nearshore area where model results are reported.

wave conditions and compare this disturbance expected as a result of storm conditions.

2.3. SWAN model implementation—Parameters and outputs

Due to the size of the computational grid, model simulations were nested to reduce computational time without sacrificing resolution. For each wind/wave scenario a model simulation was performed for the entire computational area using a 30 m resolution grid (obtained by interpolating the 2 m resolution input files to 30 m resolution in ArcMAP). The coarse-scale model was used to define boundary wave conditions (wave frequency spectra and directions) for 14 smaller 2 m resolution nearshore simulations covering the nearshore model area (Fig. 1). This ensures that high resolution results are obtained for nearshore areas without having to perform time-consuming high-resolution simulations over larger areas.

SWAN model simulations were performed in generation three mode, enabling the simulation of wave energy loss through depth-induced wave breaking, whitecapping and bottom friction (Booij et al., 1999). Triad wave-wave interactions were also activated, which in shallow water transfer wave energy from lower frequencies to higher frequencies (shorter wavelengths), particularly as waves propagate across submerged reefs (Beji and Battjes, 1992; Ris et al., 1999). Bottom friction was set to the JONSWAP formulation (alternate formulations for bottom friction and wind-wave interactions were also trialled to examine model sensitivity - see Supplementary material). The SWAN model provides results for a variety of wave parameters that can be output for each modelled grid cell such that maps, representing the spatial variation in wave parameters, can be constructed. For each wave class, gridded representations of significant wave height, wavelength, wave period and a wave-breaking parameter, Q_b, representative of the fraction of waves that have broken (Battjes and Janssen, 1978), were extracted.

2.4. Predicting wave-induced disturbance for E. radiata and M. pyrifera

Wave model output parameters were used to inform biomechanical assessments of how waves influence *E. radiata* and *M. pyrifera* (Fig. 2). Utter and Denny (1996) developed a biomechanical model for *M. pyrifera*, which relates wave motion to hydrodynamic forces acting on a *M. pyrifera* plant (Fig. 2—panel B) and how this translates to the probability of stipe failure. A brief description of the biomechanical model is given here, but for a complete description see Utter and Denny (1996).

Table 1
Description of the wind and wave regimes modelled for the Wellington south coast wave model.

Class	Range of values for each class				Averaged parameters used as boundary conditions					Frequency (% of time)
	Waves		Wind		Wind		Waves			
	Direction (° from N)	Height (m)	Direction (° from N)	Speed ($m\,s^{-1}$)	Speed ($m\,s^{-1}$)	Direction (° from N)	Height (m)	Direction (° from N)	Period (s)	
18	165–195	2–3	140–210	10–15	12.20	181.88	2.41	178.69	8.57	4.9
21	165–195	4–5	175–215	>15	17.00	198.68	4.32	178.07	10.22	0.3

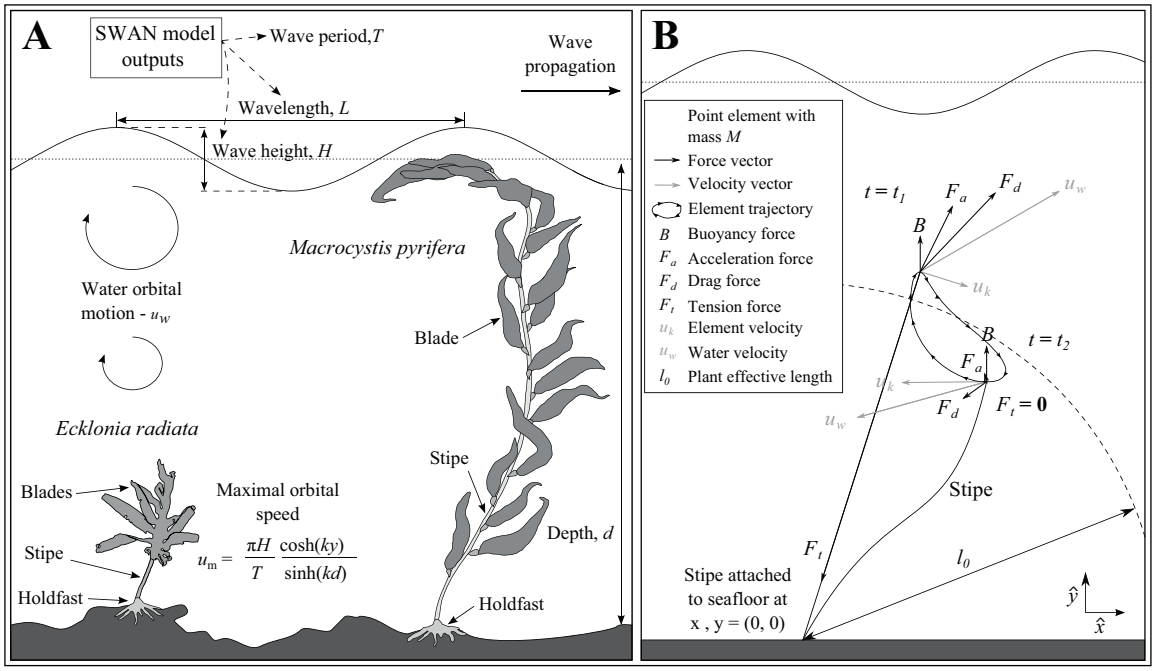

Fig. 2. Diagrams illustrating: (A) the outputs of the SWAN wave model and how they relate to wave orbital motion as well as diagrams illustrating the growth forms of *Ecklonia radiata* and a single *Macrocystis pyrifera* frond (not to scale) and (B) an illustration of the biomechanical model for *M. pyrifera*, which represents a *M. pyrifera* plant as a point element, with mass *M*, tethered to the seabed by a length of material with similar properties to a *M. pyrifera* stipe. Forces acting on the point element, as well as water and element velocities, are illustrated for two distinct time points; t_1 where tension force is maximised and t_2 where the stipe is un-stretched and tension force is zero.

Objects contained within an accelerating fluid are subjected to drag, $\boldsymbol{F_d}$, and acceleration, $\boldsymbol{F_a}$, forces (model components in bold font represent vector quantities) due to water velocity and acceleration relative to the object, respectively, and a buoyancy force, $\boldsymbol{B}$ (Gaylord et al., 1994; Utter and Denny, 1996—illustrated in Fig. 2). Utter and Denny (1996) model a *M. pyrifera* plant as a point element, with mass *M*, upon which all of the hydrodynamic forces act (Fig. 2). The point element is tethered to the seabed by a length of material, analogous to a *M. pyrifera* stipe. The hydrodynamic forces are given as:

$$\boldsymbol{B} = -gV(\rho_k - \rho_w) \tag{1}$$

$$\boldsymbol{F_a} = \rho_w C_a V \boldsymbol{a_r} + \rho_w V \boldsymbol{a_w} \tag{2}$$

$$\boldsymbol{F_d} = 0.0074 \rho_w \boldsymbol{u_r}^{1.596} A \tag{3}$$

where $\boldsymbol{a_r}$ is the acceleration of the point element ($\boldsymbol{a_k}$) relative to the acceleration of the surrounding water, $\boldsymbol{a_w}$ ($\boldsymbol{a_r} = \boldsymbol{a_w} - \boldsymbol{a_k}$), $\boldsymbol{u_r}$ is the velocity of the point element ($\boldsymbol{u_k}$), relative to the velocity of the surrounding water, $\boldsymbol{u_w}$ ($\boldsymbol{u_r} = \boldsymbol{u_w} - \boldsymbol{u_k}$) and ρ_k is the overall density of the *M. pyrifera* plant (all other terms are defined in Table 2 and parameters directly quoted as numerical values are either accepted physical constants or values measured/derived empirically by Utter and Denny, 1996). Buoyancy was assumed to be a constant (2.49 N) as found by Utter and Denny (1996).

Hydrodynamic forces act to extend the stipe creating tension, $\boldsymbol{F_t}$ (Fig. 2). Tension is determined by the departure of the plant length from its un-stretched length and is given by

$$\boldsymbol{F_t} = -\left\{ 1.91 \times 10^7 \left[\frac{\sqrt{x^2 + y^2} - l_0}{l_0} \right]^{1.407} A_{xs} \right\} \left[\cos(\theta)\,\hat{\boldsymbol{x}} + \sin(\theta)\,\hat{\boldsymbol{y}} \right] \text{ when } \sqrt{x^2 + y^2} > l_0$$

$$\boldsymbol{F_t} = 0 \text{ when } \sqrt{x^2 + y^2} \le l_0 \tag{4}$$

Table 2
Parameter values and empirical relationships used to define quantities in the force balance equation describing the wave-induced motion of a *M. pyrifera* plant. All values and relationships are taken/derived from Utter and Denny (1996).

Parameter	Explanation	Value/Relationship
H_s	Significant wave height (m)	Wave model output
T	Wave period (s)	Wave model output
L	Wave length (m)	Wave model output
d	Depth (m)	From bathymetry
k	Wavenumber	$2\pi/L$
ω	Angular wave frequency	$2\pi/T$
l	Plant length (m)	d
l_0	Effective plant length (m)	$0.8l$
A	Maximal projected area (m^2)	$A = 0.297l^{0.955}$
M	Plant mass (kg)	$0.774A$
M_e	Effective plant mass (kg)	$M_e = M + \rho_w C_a V$
V	Plant volume (m^3)	$\left(M + \left(B/g\right)\right)/\rho_w$
C_a	Added mass coefficient	3
ρ_w	Seawater density	1025 kg m^{-3}
B	Buoyancy force (magnitude)	2.49 N
g	Acceleration due to gravity	9.81 m s^{-1}
A_{xs}	Stipe cross sectional area	4.1×10^{-5} m^2

where x and y are the horizontal and vertical distances of the point mass from the seabed attachment point of the stipe, and $\hat{\boldsymbol{x}}$ and $\hat{\boldsymbol{y}}$ are unit vectors in the horizontal and vertical directions, respectively. Tension force is directed along the stipe at an angle θ with respect to the horizontal

$$\theta = \arctan\left(\frac{y}{x}\right) \tag{5}$$

The motion of the plant is governed by the interaction of the wave-induced velocity and acceleration with the plants velocity, acceleration and position. Wave-induced velocity, $\boldsymbol{u_w}$, and acceleration, $\boldsymbol{a_w}$, are related to depth (d), wave height (H), period (T) and wavelength (L) and varies as a function of time, t,

and position:

$$\boldsymbol{u_w} = \frac{\pi H}{T}\cos(kx-\omega t)\frac{\cosh(ky)}{\sinh(kd)}\hat{\boldsymbol{x}} + \frac{\pi H}{T}\sin(kx-\omega t)\frac{\sinh(ky)}{\sinh(kd)}\hat{\boldsymbol{y}} \quad (6)$$

$$\boldsymbol{a_w} = \frac{2\pi^2 H}{T^2}\sin(kx-\omega t)\frac{\cosh(ky)}{\sinh(kd)}\hat{\boldsymbol{x}} - \frac{2\pi^2 H}{T^2}\cos(kx-\omega t)\frac{\sinh(ky)}{\sinh(kd)}\hat{\boldsymbol{y}} \quad (7)$$

The force balance equation describes the acceleration of the point mass, $\boldsymbol{a_k}$, as a result of the summed hydrodynamic and tension forces:

$$M_e\boldsymbol{a_k} = \boldsymbol{B} + \boldsymbol{F_d} + \boldsymbol{F_a} + \boldsymbol{F_t} \quad (8)$$

The time dependent velocity and position of the point element was solved for by integrating the horizontal and vertical components of equation 8 using a Runge–Kutta numerical integration. The integration was started at $t = 0$, with the point element assumed to start at a position of $x = 0$, and y determined by the stretched length of the stipe assuming only buoyancy. A time step of 0.02 s was used for the numerical integration (see Supplementary material for assessment of other time steps), which was performed for 20 wave periods, and the maximum tension force, F_{max}, recorded.

The biomechanical model was parameterised by the wave model predicted values for significant waveheight, wave period and wave length, in conjunction with depth (all of which varied among locations). Plant length, l, was assumed to be equal to water depth (Utter and Denny, 1996) and only scenarios with depth between 3 and 20 m were evaluated. Because significant wave height is the average height of the highest 1/3 of all waves, the maximum wave height can be considerably larger (Utter and Denny, 1996). Within a time period, τ, the maximum wave height, H_m, for a given significant wave height, H_s, with period T can be approximated by

$$H_m = 0.6541\left\{\sqrt{\ln(\tau+T)} + 0.2886\left[\frac{1}{\sqrt{\ln(\tau/T)}}\right]\right\}H_s \quad (9)$$

For biomechanical model simulations significant wave heights were converted to maximum wave heights assuming an observation period of 3 h (resolution of the wind-wave data) over which these conditions could be considered to be approximately constant. However, waves greater than 0.78 times the local water depth are likely to have already broken due to interaction with the seabed. Therefore, if H_m exceeded 0.78 d the maximum wave height was replaced by the theoretical maximum of 0.78 d (Utter and Denny, 1996).

Evaluating every realised set of parameters of the biomechanical model (depth, H_s, T and L) was not feasible given the number of unique parameter combinations. However, many locations had similar parameters (i.e. adjacent cells) and therefore evaluating every possible combination was unnecessary. To reduce the number of unique variable combinations some simplifications were made by rounding the values for depth, H_s, T and L (see Supplementary material). Every realised combination of the rounded values for depth, H_s, T and L was identified and these values used to parameterise the biomechanical model simulations. Values for maximum tension force resulting from the biomechanical model simulations were then re-assigned to the corresponding locations to produce a gridded representation of maximum tension force across the Wellington south coast for both wave scenarios.

The empirically derived probability of a *M. pyrifera* stipe having a breaking stress less than σ, where

$$\sigma = \frac{F_{max}}{A_{xs}} \quad (10)$$

is given by $P(\sigma)$:

$$P(\sigma) = 1 - \exp\left[-\left(\frac{\sigma - 1}{3.16\times 10^6}\right)^{3.75}\right] \quad (11)$$

Maximum tension force, F_{max}, was converted to mechanical stress, which was subsequently used to calculate the probability of stipe failure. Stipe failure probabilities were evaluated for all locations including areas where *M. pyrifera* was recorded as absent. This was to provide a comparison of stipe failure probabilities among locations to evaluate whether *M. pyrifera* was potentially excluded from some locations due to an elevated chance of mortality. Maps of the spatial distribution of stipe breakage probability were produced and the numerical distribution of breakage probabilities in each of four 5 m depth intervals was examined for locations with appropriate substrates (i.e. excluding sand).

A biomechanical model for *E. radiata* was not available, but Thomsen et al. (2004) showed that *E. radiata* can be dislodged or damaged at orbital speeds >2 m s^{-1}. To identify the areas where this limit may be exceeded, maximum orbital speeds, u_m, for each wave class were calculated according to (modified from Eq. (6))

$$u_m = \frac{\pi H}{T}\frac{\cosh(ky)}{\sinh(kd)} \quad (12)$$

Orbital speeds were calculated for a height of 1 m above the substrate (i.e. $y = 1$ in Eq. (12)) to match the height at which *E. radiata* canopies, and therefore the centre of drag, are likely to occur (average total length of *E. radiata* ~93.3 cm—Wernberg et al., 2003). The spatial distribution of reef area where u_m exceeded 2 m s^{-1} was evaluated for each wind/wave scenario and the characteristics of these locations identified. Furthermore, to examine the range of orbital speeds in different depth strata, the numerical distribution of orbital speeds predicted for each wind/wave scenario were examined in 5 m depth intervals.

2.5. Relating predicted disturbance to observed macroalgal distributions

E. radiata in this area is known to be relatively widespread at depths of 7–15 m (Choat and Schiel, 1982; Schiel, 1990), so particular attention is given to the disturbance probabilities predicted at these depths. However, due to the lack of detailed information about its exact distribution no further analyses relating distribution to predicted disturbance could be performed. The distribution of large stands of *M. pyrifera* were identifiable from aerial photography as fronds were visible floating on the surface. This distribution was mapped by tracing these areas using ArcGIS. In addition, the present day distribution was qualitatively compared to that given in Figure 4 of Hay (1990) to evaluate whether *M. pyrifera* distributions in this area are approximately stable through time rather than a result of recent disturbance.

To quantitatively examine the relationship between the observed presence of *M. pyrifera* and predicted disturbance, 20,000 points were randomly placed within the 3–20 m depth interval in areas of suitable substrate (excluding sand). For each point, the predicted probabilities of stipe failure for each wave class (P_{C18} and P_{C21}), depth and the wave-breaking parameters for each wave class (Q_{C18} and Q_{C21}) was recorded in addition to the presence/absence of *M. pyrifera*. Wave breaking parameters were included in the models because water velocities associated with breaking waves can be considerably larger than in unbroken waves (Utter and Denny,

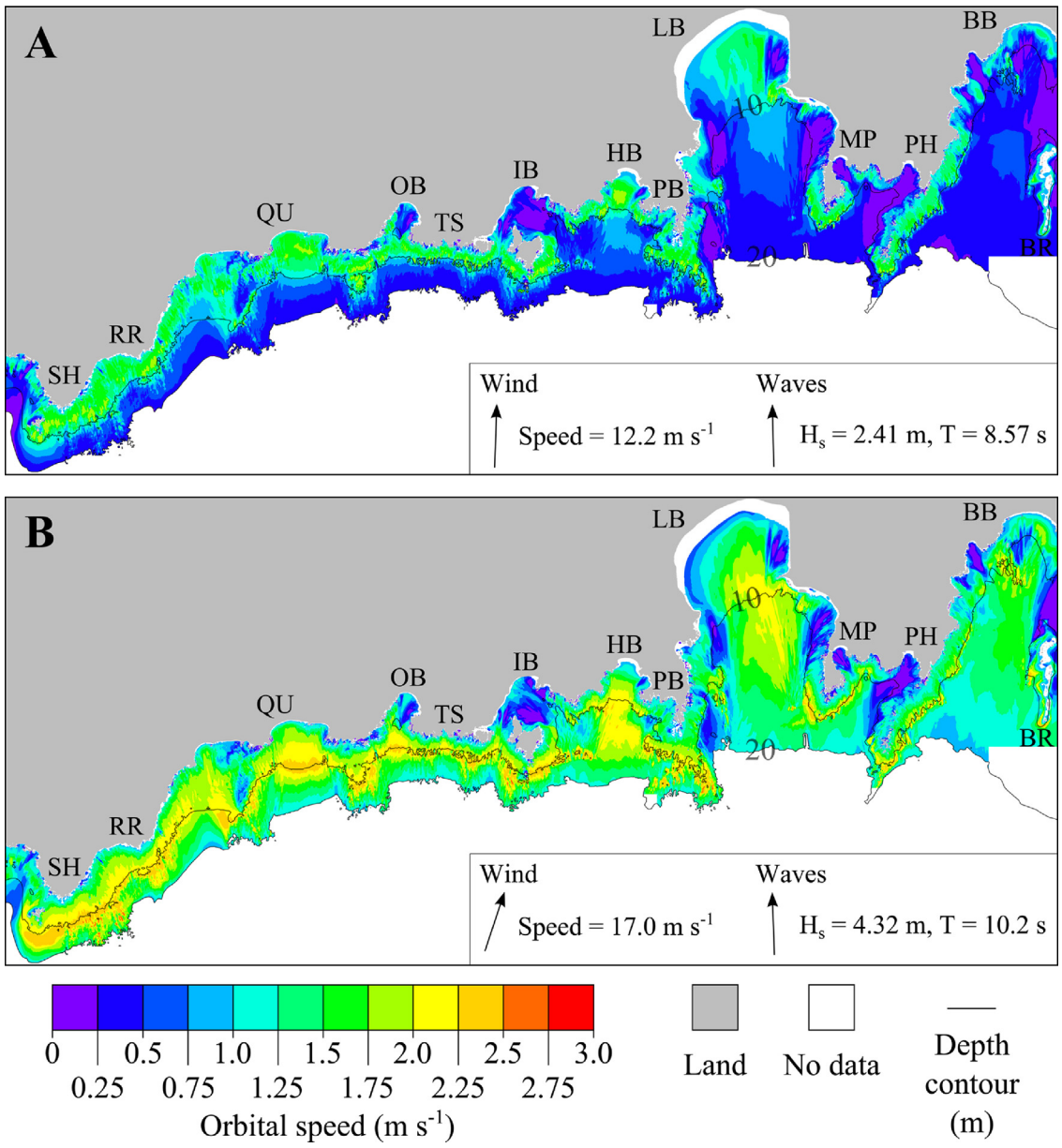

Fig. 3. Maps illustrating the predicted variation in the orbital speed 1 m above the seafloor across Wellington's south coast for (A) wave class 18 (H_{sig} = 2.41 m, T = 8.57 s, wind speed = 12.2 m s^{-1}) and (B) wave class 21 (H_{sig} = 4.32 m, T = 10.22 s, wind speed = 17 m s^{-1}). Text represents location name abbreviations: BB—Breaker Bay, BR—Barrett Reef, PH—Palmer Head, MP—Moa Point, LB—Lyall Bay, PB—Princess Bay, HB—Houghton Bay, IB—Island Bay, TS—The Sirens, OB—Owhiro Bay, QU—Quarry, RR—Red Rocks, SH—Sinclair Head.

1996), which may have the effect of excluding plants from surf-zone locations. A binomial generalised linear model (GLM) was fitted to the resulting presence/absence data with depth, P_{C18}, P_{C21}, Q_{C18} and Q_{C21} as continuous predictors. Breaking parameters, Q_{C18} and Q_{C21}, were closely correlated (pearsons correlation coefficient of 0.85) and so were not included in the same models, but trialled against each other to identify which provided the better fit to the data. All possible model combinations of these factors were trialled and ranked by AIC to identify the model that best described *M. pyrifera* presence/absence. To account for non-linear responses to the model predictors, the same procedure was applied as for GLMs, but using generalised additive models (GAMs) specifying the response as a smooth function of the predictor variables. All biomechanical model simulations and analyses were performed in R version 2.15 (R Core Team, 2013).

3. Results

3.1. *Subtidal orbital velocity and potential impacts on* E. radiata

Orbital speeds 1 m above the seabed were predicted to range from 0 to 2.05 m s^{-1} for regular wave conditions (wave class 18), and 0–2.71 m s^{-1} for storm conditions (wave class 21), and varied considerably among locations (Fig. 3 and Table 3). The lowest orbital speeds were predicted for locations directly behind obstacles (e.g. in the lee of islands, island groups and shallow submerged reefs), whereas the highest orbital speeds were predicted for submerged obstacles directly exposed to incoming waves (e.g., shallow submerged reefs and around emergent reefs such as at Palmer Head and Barrett Reef) and in the surf zone along several beaches and bays (Fig. 3).

Table 3
Summary of the wave model predicted orbital speeds at 1 m above the seafloor. Values correspond to the % area experiencing orbital speeds within each of six discrete speed ranges. Results are given for both modelled wave classes in four depth intervals for rocky reef substrata. In addition, the maximum, median and range (range capturing 90% of the predicted values) of orbital speed predicted for each wave class, depth interval and substrate type is also presented. Values left blank correspond to zero.

Wave class	Depth range (m)	Percent area in orbital speed range						Max orbital speed ($m\,s^{-1}$)	Median orbital speed ($m\,s^{-1}$)	90% range of orbital speed ($m\,s^{-1}$)
		0–0.5 $m\,s^{-1}$	0.5–1 $m\,s^{-1}$	1–1.5 $m\,s^{-1}$	1.5–2 $m\,s^{-1}$	2–2.5 $m\,s^{-1}$	2.5–3 $m\,s^{-1}$			
C18	0–5	10.73	25.06	48.43	15.79			1.94	1.15	0.28–1.61
	5–10	9.33	15.48	40.28	34.87	0.03		2.05	1.33	0.28–1.8
	10–15	16.58	67.88	15.51	0.03			1.68	0.72	0.2–1.17
	15–20	81.47	18.53					0.92	0.4	0.26–0.59
C21	0–5	6.35	23.57	51.66	18.39	0.03		2.09	1.17	0.43–1.72
	5–10	3.07	5.32	9.79	45.13	36.69	0.01	2.58	1.92	0.71–2.26
	10–15	4.02	5.41	9.69	35.77	44.26	0.84	2.71	1.94	0.63–2.39
	15–20	1.73	4.42	59.09	32.88	1.87	0.02	2.66	1.39	0.97–1.87

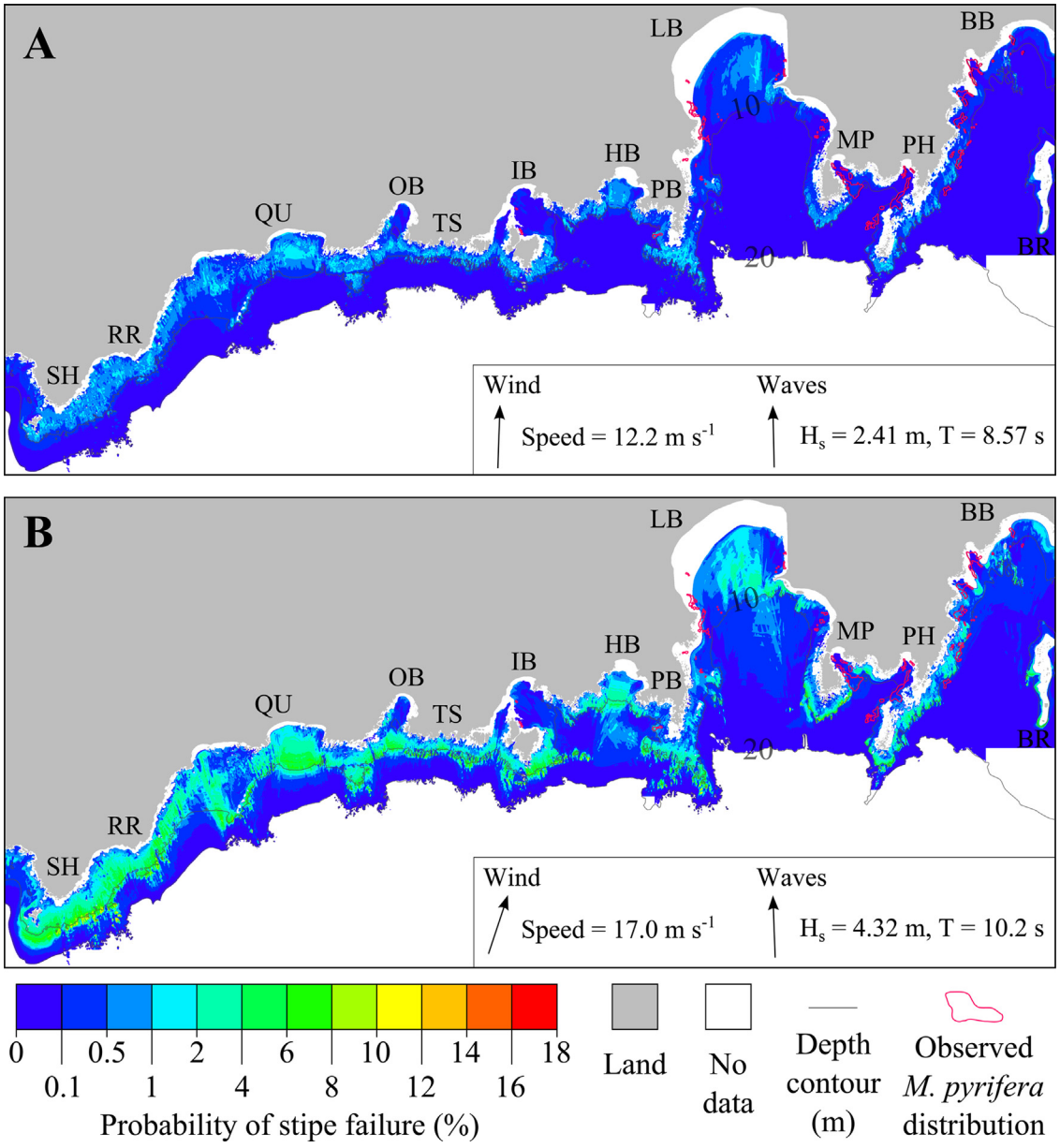

Fig. 4. Maps illustrating the observed distribution of *M. pyrifera* and the variation in the computed probability of *M. pyrifera* stipe failure along Wellington's south coast for (A) wave class 18 (H_{sig} = 2.41 m, T = 8.57 s, wind speed = 12.2 $m\,s^{-1}$) and (B) wave class 21 (H_{sig} = 4.32 m, T = 10.22 s, wind speed = 17 $m\,s^{-1}$). Abbreviations of location names are BB—Breaker Bay, BR—Barrett Reef, PH—Palmer Head, MP—Moa Point, LB—Lyall Bay, PB—Princess Bay, HB—Houghton Bay, IB—Island Bay, TS—The Sirens, OB—Owhiro Bay, QU—Quarry, RR—Red Rocks, SH—Sinclair Head.

Table 4
Summary of the biomechanical model predicted probabilities of stipe failure (P_{fail}) for *M. pyrifera*. Values correspond to the % area predicted to have stipe failure probabilities within each of seven discrete intervals. Results are given for both modelled wave classes in four depth intervals. In addition, the maximum, median and range (range capturing 90% of the predicted values) of the predicted stipe failure probabilities predicted for each wave class in each depth interval is also presented. Values left blank correspond to zero.

Wave class	Depth range (m)	Percent area in P_{fail} range							Max P_{fail} (%)	Median P_{fail} (%)	90% range of P_{fail} (%)
		0–0.1 (%)	0.1–0.5 (%)	0.5–1 (%)	1–5 (%)	5–10 (%)	10–15 (%)	15–20 (%)			
C18	3–5	15.88	49.67	29.2	5.25				3.02	0.34	0.03–1.01
	5–10	18.17	40.29	31.7	9.84				2.56	0.37	0.05–1.11
	10–15	86.92	13.04	0.04					0.62	0.04	0.01–0.19
	15–20	100							0.02	2×10^{-3}	$(1–4) \times 10^{-3}$
C21	3–5	5.77	23.95	39.45	30.7	0.13			7.85	0.76	0.08–2.42
	5–10	5.30	28.25	13.41	45.48	7.44	0.12	0	16.56	1.19	0.1–5.61
	10–15	27.94	42.65	9.24	14.91	4.91	0.34	0.01	17.23	0.21	0.04–5.15
	15–20	86.93	12.39	0.52	0.16				4.53	0.03	0.01–0.18

Table 5
Depth, biomechanical (P_{fail}—probability of stipe failure) and wave-breaking parameter (Q—% of waves that have broken) statistics from locations where *M. pyrifera* was recorded as present, and from locations where *M. pyrifera* was absent. C18 and C21 refer to results obtained for wave model simulations of wind/wave class 18 and 21, respectively.

Factor	Present				Absent			
	Mean	Median	Max	90% range	Mean	Median	Max	90% range
Depth	6.6	5.4	16.0	3.3–12.9	10.8	10.4	20.0	3.5–19.0
P_{fail} (C18)	0.15	0.09	1.16	0.01–0.56	0.23	0.07	3.02	0.00–0.95
P_{fail} (C21)	0.43	0.28	5.43	0.04–1.28	0.99	0.32	17.23	0.01–4.44
Q (C18)	0.05	0	6.85	0–0.23	0.26	0	100	0–1.13
Q (C21)	0.57	0.00	49.43	0–2.67	1.43	0.00	100	0–7.43

The spread of orbital speeds varied with depth, with the highest orbital speeds and the largest range in values observed in the 5–10 m depth interval for regular wave conditions, but in the 10–15 m depth interval for storm conditions (Table 3). This is likely due to waves breaking at different depths under the different modelled conditions, with larger waves tending to break in deeper water (i.e. in the 10–15 m depth interval for storm conditions) than smaller waves (i.e. waves breaking in the 5–10 m depth interval for the smaller waves modelled for regular wave conditions), dissipating much of their energy in the process. For both wave conditions investigated, orbital speeds in the 0–5 m depth interval were markedly similar, also potentially due to the fact that in both cases the largest waves have already broken before reaching the 5 m depth contour.

For *E. radiata* the critical speed defined by Thomsen et al. (2004) of 2 m s^{-1} was only exceeded over a small area (0.03% of the 5–10 m depth interval—Table 3) under regular wave conditions at locations with depths of 5–7 m. These areas tended to be confined to the tips of submerged reefs, which present the first obstacle to incoming waves (Fig. 3). Under storm conditions, extensive areas in the 5–15 m depth interval were predicted to experience orbital speeds in excess of 2 m s^{-1} (Fig. 3), with ~35–45% of all rocky reef areas in this depth range predicted to experience potentially damaging wave forces (Table 3). However, in the majority of locations this limit is only exceeded by 0.2–0.4 m s^{-1}, with a small proportion of areas (0.84% of the 10–15 m depth interval) expected to experience orbital speeds in excess of 2.5 m s^{-1} (Table 3). The spatial distribution of potentially damaging orbital speeds also differs between the east-end of the modelled area (east of Princess Bay/Houghton Bay), which in general appears less exposed, and the west-end, which appears more exposed (Fig. 3). In particular, most areas at depths of 7–13 m west of Princess Bay were predicted to experience orbital speeds in excess of 2 m s^{-1} during storms with the most exposed locations predicted to be between Red Rocks and Sinclair Head (Fig. 3).

3.2. *Predicted disturbance of* M. pyrifera *and relationship with observed distribution*

The distribution of *M. pyrifera*, identified from aerial photography, closely matches the distribution identified by Hay (1990) for *M. pyrifera* along the Wellington south coast (Fig. 4 of that paper), indicating that observed patterns are representative of its long-term distribution (at least over a 20 year timescale), rather than being a result of recent disturbances/recruitment. The majority of *M. pyrifera* was observed along the coastline in Breaker Bay, behind Palmer Head reef to Moa Point and a few scattered stands along the coastline leading into and out of Lyall Bay (Figs. 4 and 5).

Stipe failure probabilities were predominantly <15% across the majority of the modelled area for both wave scenarios modelled (Fig. 4). The spatial distribution of stipe failure probabilities was similar to bottom orbital speed, with locations at the tips of reefs and open sections of coastline predicted to have relatively higher stipe failure rates than more sheltered locations within bays and behind emergent reefs and/or islands (Figs. 4 and 5). Under regular wave conditions the maximum stipe failure probability was predicted to be 3%, with less than 10% of the area between 3 and 10 m deep predicted to have probabilities of failure greater than 1% (Table 4). Areas with a predicted stipe failure rate of 1% or higher under regular wave conditions tended to be on exposed rocky reefs at depths of 4–7 m, with particular examples including reefs between Red Rocks and Sinclair Head, south of Princess Bay, at the tip of the Moa Point peninsula and south of Palmer Head (Fig. 4). No areas greater than 10 m deep were predicted to have stipe failure probabilities greater than 1% under regular storm conditions (Table 4). Under storm conditions stipe failure probabilities peaked at 17%, although probabilities of <6% were predicted for the majority of areas (Fig. 4 and Table 4). The highest stipe failure probabilities were predicted for depths of ~12–13 m on exposed reef outcroppings (Fig. 4). However, the areas associated with the most consistently high failure probabilities were in the 5–10 m depth

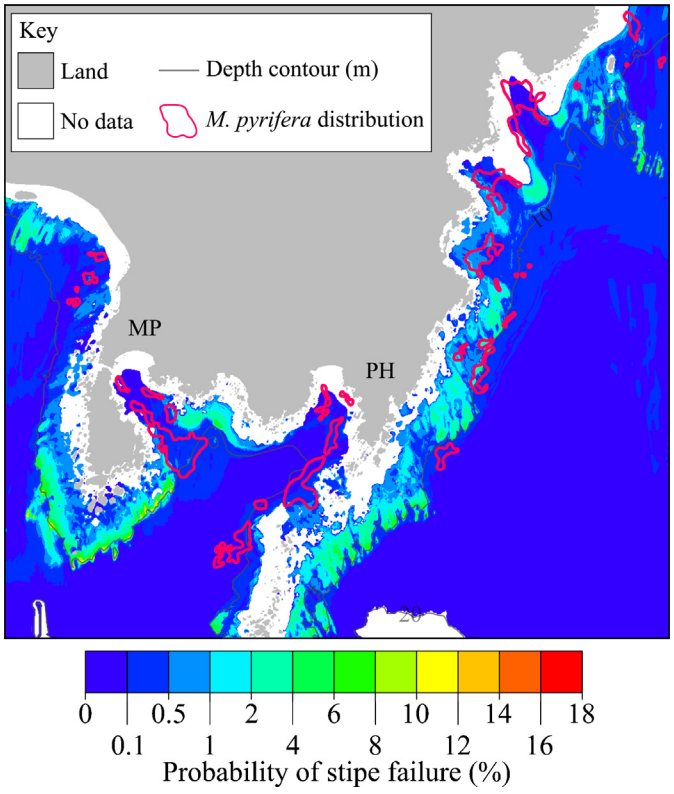

Fig. 5. A cropped portion of Fig. 4(B) illustrating the majority of the observed distribution of *M. pyrifera* in the study region in relation to the calculated probability of stipe failure. Stipe failure probabilities correspond to those calculated from wave model simulations of wave class 21 (H_{sig} = 4.32 m, T = 10.22 s, wind speed = 17 m s^{-1}). Abbreviations of location names are: PH—Palmer Head and MP—Moa Point.

interval where greater than half of the area was predicted to have probabilities greater than 1%, compared to one fifth of the area in the 10–15 m depth interval (Table 4). At depths greater than 15 m failure rates were considerably lower, with failure rates of less than 0.5% predicted for the majority (99%) of the area between 15 and 20 m deep (Table 4). Similarly areas shallower than 5 m were also predicted to have lower failure rates, likely as a result of reduced plant size modelled at these depths (Table 4).

Examination of predicted wave conditions at locations where *M. pyrifera* was present revealed that these locations tended to have lower predicted stipe failure rates (<1.3% chance of stipe failure in the majority of locations even under storm conditions—Fig. 5) and were in locations where the majority of waves have yet to break (lower Q value), when compared to locations where *M. pyrifera*

Table 6
Model description and AIC statistics for binomial generalised linear and generalised additive model fits to the *M. pyrifera* presence/absence data with depth, probability of stipe failure (P_{fail}) and wave-breaking parameters (Q—% of waves that have broken) as predictors. C18 and C21 refer to the results obtained for wave model simulations of wind/wave class 18 and 21, respectively.

Model type	Model factors	AIC	Akaike weight
GLM	Depth + P_{fail} (C18) + P_{fail} (C21) + Q (C18)	1905.2	0.991
	Depth + P_{fail} (C21) + Q (C18)	1915.9	0.005
	Depth + P_{fail} (C18) + P_{fail} (C21) + Q (C21)	1916.1	0.004
GAM	Depth + P_{fail} (C18) + P_{fail} (C21) + Q (C18)	1896.5	0.921
	Depth + P_{fail} (C18) + P_{fail} (C21) + Q (C21)	1902.4	0.048
	Depth + P_{fail} (C21) + Q (C18)	1903.4	0.029

was recorded as absent (Table 5). The best-fitting GLM and GAM models (lowest AIC) to the *M. pyrifera* presence-absence data had the same model components, including terms for depth, stipe failure probability for both wave conditions and the wave-breaking parameter for regular wave conditions (Table 6). All GLM model coefficients were significantly negative (95% CI not overlapping with zero) indicating that increases in depth, probability of stipe failure and wave-breaking parameter were correlated with a decreased probability of *M. pyrifera* presence (Table 7). Generalised additive models of *M. pyrifera* presence/absence had lower AIC statistics than the corresponding linear models, indicating that there were some non-linear relationships between predictors and the probability of *M. pyrifera* presence (Table 6). Upon examination, the fitted relationships were similar for all factors between GLM and GAM fits to the data (Fig. 6), with linear (EDF = 1—Table 7), rather than non-linear, terms fitted for P_{C18}, P_{C21} and Q_{C18}. The fitted GAM response for depth was non-linear (EDF = 2.4—Table 7) and for low depths (<10 m) the relationship was less steep than the GLM fit, indicating that *M. pyrifera* prevalence doesn't decline with depth as steeply as indicated by the GLM, but both model predictions converged for depths ≥13 m (Fig. 6).

4. Discussion

Identifying factors that govern the distribution and abundance of species is important if we are to understand species' distributions, and the mechanisms that drive these distributions (Kearney and Porter, 2009). This study demonstrates the utility of models for predicting the spatial distribution of physical factors, and illustrates how this information can be combined with known physiological/biomechanical relationships in an effort to understand rates of disturbance and how they may relate to species distributions. In addition, this study provides a link between two fields of study that have typically been applied at different scales (macroalgal

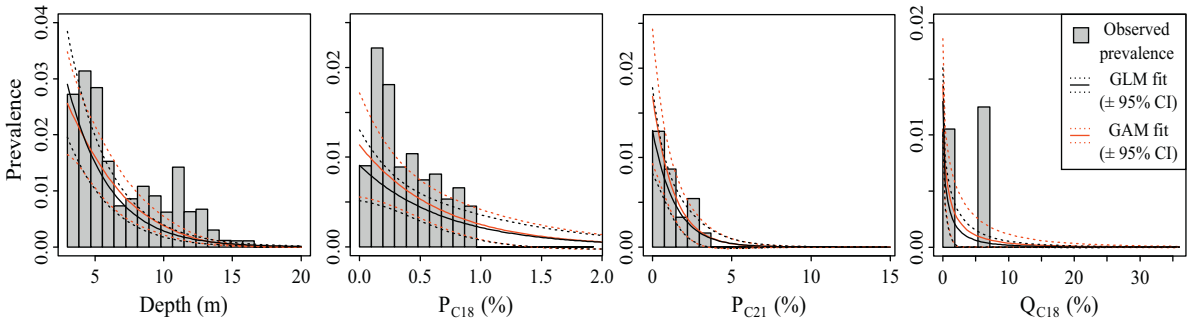

Fig. 6. Graphs illustrating the observed prevalence of *M. pyrifera* in relation to depth, the predicted probability of stipe failure for each wave class (P_{C18} and P_{C21}) and a wave-breaking parameter for wave class 18 (Q_{C18}). Lines represent the binomial logistic regression line for generalised linear (GLM) and generalised additive model (GAM) fits to the data, calculated for each predictor holding the other predictors at their mean value. For illustration purposes filled bars indicate the mean observed prevalence of *M. pyrifera* in 20 equally spaced intervals along the x-axis for each predictor.

Table 7
Binomial generalised linear model coefficients (mean and 95% confidence interval) and generalised additive model statistics (EDF—effective degrees of freedom, Chi-squared statistic and approximate significance of the fitted smooth term) for the best fitting (lowest AIC) models to the *M. pyrifera* presence absence data with depth, probability of stipe failure (P_{fail}) and wave-breaking parameters (Q—% of waves that have broken) as predictors. C18 and C21 refer to the results obtained for wave model simulations of wind/wave class 18 and 21, respectively.

Factor	GLM coefficients		GAM statistics		
	Estimate	95% CI	EDF	Chi-Sq	*p*-Value
(Intercept)	−0.8	[−1.2, −0.4]			
Depth	−0.3	[−0.4, −0.3]	2.4	198.6	$<2\times10^{-16}$
P_{fail} (C18)	−144.9	[−235, −63]	1	11.5	7×10^{-4}
P_{fail} (C21)	−71.0	[−105, −42]	1.0	21.6	3×10^{-6}
Q (C18)	−13.7	[−21.1, −7.5]	1.0	11.7	6×10^{-4}

biomechanics often evaluated on an individual level versus wave modelling that is concerned with large-scale variability in wave-forces), to identify consequences of wave forces on macroalgae at a geographic level. Our results suggest that regularly occurring wave conditions are unlikely to cause damage to healthy *E. radiata* plants, while considerable disturbance may occur over wide areas as a result of storm events. For both scenarios investigated low mortality rates were predicted for *M. pyrifera* plants across the entire modelled area. However, there was some evidence to suggest that the distribution of *M. pyrifera* along the Wellington south coast is inversely related to wave exposure as large stands of *M. pyrifera* coincided with sheltered locations, despite the low predicted probabilities of disturbance at more exposed sites.

4.1. Wave modelling and predicted disturbance patterns

Comparatively, the maximum speeds predicted by the SWAN model (2–3 m s^{-1}) were similar to maximum instantaneous wave speeds (1.5–2 m s^{-1}) measured *in situ* for locations open to waves in the northwest USA (Eckman et al., 2003), and to maximum values (~3 m s^{-1}) predicted by SWAN models for exposed locations in Western Australia (England et al., 2008). The results indicate that during storm conditions, greater than 40% of the modelled area at depths where *E. radiata* most commonly occurs (7–15 m—Choat and Schiel, 1982; Schiel, 1990) is predicted to experience orbital speeds in excess of 2 m s^{-1}. This may lead to considerable disturbance to *E. radiata* at these locations. However, in the vast majority of locations this limit was only exceeded by up to 0.4 m s^{-1}, which is likely to result in the selective removal of individuals above a certain size (because drag increases with size and projected surface area—Gaylord et al., 1994), rather than causing indiscriminate damage to all plants. This may result in a spatially variable upper size limit on *E. radiata* plants (Blanchette, 1997; Thomsen et al., 2004). The removal of the largest individuals is likely to alter canopy density, with subsequent effects on the degree of shading (Clark et al., 2004) and understorey species composition and biodiversity (Toohey et al., 2004, 2007) as well as allowing for colonisation by other *E. radiata* individuals. In contrast, *E. radiata* plants are unlikely to be damaged under regularly occurring wave conditions because only at a few locations were orbital speeds predicted to exceed 2 m s^{-1}. However, it has to be recognised that wave forces are unlikely to act in isolation. Age, damage due to herbivory, and scouring and fracturing effects due to continual wave forces may weaken individual plants (Denny et al., 1989; Mach et al., 2007). The combined effect of prior damage with sub-critical wave forces may lead to the removal of individual plants during regular wave conditions, rather than wide-scale disturbance as predicted for storm conditions.

Stipe failure rates for *M. pyrifera* are predicted to be less than 10% across the majority of locations investigated in the event of a storm. However, there was a negative correlation between prevalence of *M. pyrifera* and stipe failure rates/wave breaking parameters, suggesting that the distribution of *M. pyrifera* may be related to wave exposure in this area. In particular, *M. pyrifera* was only recorded at locations outside of the surf zone for regularly occurring wave conditions (i.e. where Q_{C18} was zero or low). Previous studies have suggested that plants caught in breaking waves are likely to be damaged due to the increased and turbulent water flow associated with wave breaking (Seymour et al., 1989; Utter and Denny, 1996). Because these conditions occur relatively frequently, the forces associated with wave breaking may act to exclude *M. pyrifera* from surf zone locations. However, alternative explanations for the distribution of *M. pyrifera*, such as due to temperature, substrate availability, nutrients and grazing must also be addressed. Suitable substrate, in the form of rocky reefs, occur throughout the area considered, but in many locations exist as small unconsolidated outcroppings that may not support large collections of *M. pyrifera* plants. Furthermore, many areas that are less exposed, particularly throughout Lyall Bay and Island Bay, are predominantly sand, which despite the lower wave exposure are not suitable for *M. pyrifera* settlement and growth. Temperature tolerance may also prevent growth at certain times as *M. pyrifera* is a cold water species and Wellington is near to the northern limit of *M. pyrifera* in New Zealand (Brown et al., 1997). However, it has been reported that summer temperatures are within the temperature limits of *M. pyrifera* (Hay, 1990), but may be sufficiently high to reduce growth rates (Dean and Jacobsen, 1984), which may affect its spatial distribution or susceptibility to wave-induced disturbance. It has been reported that *M. pyrifera* may be unable to persist in locations with nitrate concentrations lower than 1 μmol l^{-1} for sustained periods of time (Hay, 1990). Nitrate concentrations along the Wellington south coast, which are on average ~1–2 μmol l^{-1}, (Bradford et al., 1986; Hay, 1990) may contribute to limiting *M. pyrifera* growth at certain times. In addition, the majority of *M. pyrifera* in the area investigated exists in close proximity to the Wellington Harbour entrance (east of Moa Point), which may be associated with higher nutrient concentrations (Hay, 1990) allowing for greater growth potential than locations further westward. It has also been reported that urchin (*Evechinus chloroticus*) abundance, and by proxy grazing pressure, is higher at the eastern end of the area investigated (Pande and Gardner, 2009), coincident with the location of the majority of *M. pyrifera* stands. If grazers were to selectively target other macroalgal species, it may increase the availability of free space allowing *M. pyrifera* to colonise areas that would otherwise be unavailable, which may contribute to its observed distribution. These factors may also interact with each other to produce the observed distribution. Although our results support the hypothesis that the distribution of *M. pyrifera* can be attributed in part to the spatial variation of wave forces in this area, given the additional limiting factors highlighted above, it is likely not the only determining factor with further work needed to assess the conditions under which *M. pyrifera* will grow and survive in this area.

Given this assertion, however, it is necessary to address the discrepancy between the low predicted probabilities of stipe failure and the observed distribution. Comparisons between the recorded mortality rate during storms in southern California and those predicted by this biomechanical model revealed that the model vastly underestimated mortality rates, with predicted mortality rates of 0.1–26.2%, compared to observed rates of 13–94% (Seymour et al., 1989; Utter and Denny, 1996). The single largest contributor to mortality, unexplained by this model, has been attributed to stipe entanglement (Seymour et al., 1989). This has the effect of doubling or even tripling the forces on a single stipe, leading to a much higher probability of stipe failure (Seymour et al., 1989; Utter and Denny, 1996). Thus, the predicted probabilities presented here may also underestimate the overall rate of disturbance. In the event of disturbance, however, both the magnitude of disturbance and the ability to recover or re-establish determine the long-term viability of an individual or population. For small-scale disturbance it has been observed that *M. pyrifera* forests are able to quickly recover over 2–3 months to pre-disturbance levels through individual plant regrowth and recruitment (Dayton and Tegner, 1984; Byrnes et al., 2011). Individual plants that have been damaged may regrow lost material rapidly (up to 8–10 new fronds month^{-1} with frond elongation rates of 10–15 cm day^{-1} in optimal conditions, but growth may be considerably slower in New Zealand conditions—Kain, 1982; Zimmerman and Kremer, 1986) contributing significantly to kelp forest recovery (Romme et al., 1998). The biomechanical model describes the breakage of an individual stipe at its weakest point, which may leave sufficient material, either in the form of remaining fronds, or material below the break point, for rapid regrowth. However, in the event of violent disturbance, plants may lose all fronds or be sufficiently damaged that they are unable to regenerate lost material (Dayton and Tegner, 1984; Seymour et al., 1989). The loss of canopy associated with large-scale disturbance also allows colonisation by other macroalgal species, which may exclude *M. pyrifera* recruits preventing kelp forest recovery (Dayton and Tegner, 1984). In addition, the conditions at locations that are subject to frequent disturbance (e.g. surf-zone locations) may prevent a critical canopy cover from establishing, which would otherwise suppress the growth of competing macroalgal species that when present are resistant to invasion by *M. pyrifera* recruits, further reducing the ability of *M. pyrifera* to colonise these areas (Dayton and Tegner, 1984; Byrnes et al., 2011). Consequently in order for *M. pyrifera* distributions to be relatively constant on the Wellington South Coast (the current distribution matches that given in Hay, 1990), the locations where *M. pyrifera* persists must experience relatively low-levels of disturbance, which matches our model predictions for these areas.

4.2. Limitations of the approaches adopted

The application of the wave model results to the two species of macroalgae considered resulted in different levels of information regarding their distribution with respect to wave exposure. The application of an absolute limit for *E. radiata* yielded some information regarding the rates of dislodgement during winter storms, but how this applies to community or size structure is unresolved. Further work to identify whether model predictions are consistent with the spatial variation of *E. radiata* size structure would provide a vital test of these model predictions. The adoption of a biomechanical model for *M. pyrifera* provided a far greater amount of information, which was further aided by knowledge of its current distribution, allowing for some tests of the model predictions. The disadvantage of the application of biomechanical models is that they often underestimate the rates of disturbance (Mach et al., 2011), due to idealised situations that are unlikely to occur in nature. However, these models are flexible enough that some of these shortcomings can be addressed. As an example, entanglement of *M. pyrifera*, which has been associated with increased mortality rates (Seymour et al., 1989), could be applied within this model framework by modifying the mass and projected surface area such that a single stipe bears the combined hydrodynamic forces of two or more plants. This may result in more representative rates of disturbance and highlights the greater level of detail that can be obtained through the use of biomechanical models.

The application of biomechanical models do, however, require a far greater amount of information regarding plant size and morphology. In order to apply the *M. pyrifera* model to evaluate probabilities of disturbance for the modelled area we made several assumptions about the size and morphology of plants that require some further discussion. Firstly we made the assumption that *M. pyrifera* size was equal to water depth. This may not be applicable, as *M. pyrifera* may grow to exceed depth in order to increase its canopy area once it has grown to reach the water's surface (Gaylord et al., 2008). This increases the projected surface area, increasing drag, and places more of the plants mass and projected area near the surface of the water where wave-induced water speeds (in particular for breaking waves) are higher (Gaylord et al., 2008). This would have the effect of increasing the hydrodynamic forces on a *M. pyrifera* stipe, potentially increasing the probability of failure. Second, the biomechanical model was created for Californian plants, which display morphological differences to those observed from New Zealand (Kain, 1982; Nyman et al., 1993). This would likely influence the relationship between size and surface area, the location of the centre of drag, and how tension relates to mechanical stress (i.e. differences in stipe cross-sectional area) with consequences for predicted probability of stipe failure. Given these limitations and those outlined in the previous section, the predictions of stipe failure should be interpreted as giving a relative, rather than absolute measure of the probability of disturbance for this area.

4.3. Implications

The development of correlative (rather than mechanistic) marine species distribution models (SDMs) relies upon the development of suitable geographic layers of those factors that govern species distributions. This research highlights the capacity of models to predict physical factors, such as wave-action, which can be used in marine SDMs. Furthermore, developing a mechanistic understanding of where species occur, based on physiological or biomechanical constraints, may give greater ability for predicting changes to species distributions given projected changes to the physical environment (Kearney and Porter, 2009). This may be particularly important for evaluating protected area scenarios and developing marine spatial plans that are relevant given projected shifts in species distributions. In addition, the results of this study could be used to identify areas where sub-lethal damage to macroalgae as a result of human activities (e.g. fishing and boating), is more likely to result in wave-induced damage or mortality (e.g. wounds to *E. radiata* vastly increase the rate of breakage; de Bettignies et al., 2012). This information could be used to identify limited use areas (i.e. restricted boating and/or fishing types) to limit the potential for damage to macroalgal communities.

5. Conclusion

Our study details the development of a high resolution wave model to aid in the description of subtidal species communities. This represents one of the few examples (but see also England et al., 2008; Huang et al., 2012) where wave modelling has been used in an ecological context and links individual-based models of macroalgal biomechanics to the spatial distribution of wave forces

to understand the implications of biomechanical thresholds on a geographic level. Although the data requirements of wave modelling are significant, requiring the joint availability of accurate bathymetry, weather and wave information, when this information is available, the development of SWAN models can provide information that would otherwise be missing from studies of subtidal species and communities. Wave model results could also be used in future studies to understand the drivers of community dynamics along this section of coastline both temporally with regard to episodic storms events and also spatially in describing differences in species composition among locations.

Acknowledgements

We thank Ashley Rowden, Arne Pallentin and Kevin Mackay (NIWA) for providing access to the bathymetry and substrate data files. T. Jones was supported by a Victoria University of Wellington PhD scholarship.

Appendix A. Supplementary data

Supplementary data associated with this article can be found, in the online version, at http://dx.doi.org/10.1016/j.ecolmodel.2015.06.026

References

Battjes, J.A., Janssen, J.P.F.M., 1978. Energy loss and set-up due to breaking of random waves. Coast. Eng. Proc. 1, 569–587.
Beji, S., Battjes, J.A., 1992. Experimental investigation of wave propagation over a bar. Coast. Eng. 19, 151–162.
Blanchette, C.A., 1997. Size and survival of intertidal plants in response to wave action: a case study with *Fucus gardneri*. Ecology 78, 1563–1578.
Booij, N., Ris, R.C., Holthuijsen, L.H., 1999. A third-generation wave model for coastal regions: 1. Model description and validation. J. Geophys. Res. 104, 7649–7666.
Bradford, J.M., Lapennas, P.P., Murtagh, R.A., Chang, F.H., Wilkinson, V., 1986. Factors controlling summer phytoplankton production in greater Cook Strait, New Zealand. N.Z. J. Mar. Freshwater 20, 253–279.
Brown, M.T., Nyman, M.A., Keogh, J.A., Chin, N.K.M., 1997. Seasonal growth of the giant kelp *Macrocystis pyrifera* in New Zealand. Mar. Biol. 129, 417–424.
Burrows, M.T., Harvey, R., Robb, L., 2008. Wave exposure indices from digital coastlines and the prediction of rocky shore community structure. Mar. Ecol. Prog. Ser. 353, 1–12.
Burrows, M.T., 2012. Influences of wave fetch, tidal flow and ocean colour on subtidal rocky communities. Mar. Ecol. Prog. Ser. 445, 193–207.
Byrnes, J.E., Reed, D.C., Cardinale, B.J., Cavanaugh, K.C., Holbrook, S.J., Schmitt, R.J., 2011. Climate-driven increases in storm frequency simplify kelp forest food webs. Global Change Biol. 17, 2513–2524, http://dx.doi.org/10.1111/j.1365-2486.2011.02409.x
Carrington-Bell, E., Denny, M.W., 1994. Quantifying wave exposure: a simple device for recording maximum velocity and results of its use at several field sites. J. Exp. Mar. Biol. Ecol. 181, 9–29.
Carter, L., Heath, R.A., 1975. Role of mean circulation, tides, and waves in the transport of bottom sediment on the New Zealand continental shelf. N.Z. J. Mar. Freshwater 9, 423–448.
Carter, L., Lewis, K., 1995. Variability of the modern sand cover on a tide and storm driven inner shelf, south Wellington, New Zealand. N.Z. J. Geol. Geophys. 38, 451–470.
Choat, J.H., Schiel, D.R., 1982. Patterns of distribution and abundance of large brown algae and invertebrate herbivores in subtidal regions of northern New Zealand. J. Exp. Mar. Biol. Ecol. 60, 129–162.
Clark, R.P., Edwards, M.S., Foster, M.S., 2004. Effects of shade from multiple kelp canopies on an understorey algal assemblage. Mar. Ecol. Prog. Ser. 267, 107–119.
Dayton, P.K., Tegner, M.J., 1984. Catastrophic storms, El Niño, and patch stability in a southern California kelp community. Science 224, 283–285.
de Bettignies, T., Thomsen, M.S., Wernberg, T., 2012. Wounded kelps: patterns and susceptibility to breakage. Aquat. Biol. 17, 223–233.
Dean, T.A., Jacobsen, F.R., 1984. Growth of juvenile *Macrocystis pyrifera* (Laminariales) in relation to environmental factors. Mar. Biol. 83, 301–311.
Denny, M.W., Brown, V., Carrington, E., Kraemer, G., Miller, A., 1989. Fracture mechanics and the survival of wave-swept macroalgae. J. Exp. Mar. Biol. Ecol. 127, 211–228.
Denny, M.W., Gaylord, B., 2002. The mechanics of wave-swept algae. J. Exp. Biol. 205, 1355–1362.
Denny, M.W., Gaylord, B., 2010. Marine ecomechanics. Annu. Rev. Mar. Sci. 2, 89–114.
Duggins, D.O., Eckman, J.E., Siddon, C.E., Klinger, T., 2003. Population, morphometric and biomechanical studies of three understorey kelps along a hydrodynamic gradient. Mar. Ecol. Prog. Ser. 265, 57–76.
Eckman, J.E., Duggins, D.O., Siddon, C.E., 2003. Current and wave dynamics in the shallow subtidal: implications to the ecology of understorey and surface-canopy kelps. Mar. Ecol. Prog. Ser. 265, 45–56.
Elith, J., Leathwick, J.R., 2009. Species distribution models: ecological explanation and prediction across space and time. Ann. Rev. Ecol. Evol. Syst. 40, 677–697.
England, P.R., Phillips, J., Waring, J.R., Symonds, G., Babcock, R., 2008. Modelling wave-induced disturbance in highly biodiverse marine macroalgal communities: support for the intermediate disturbance hypothesis. Mar. Freshwater Res. 59, 515–520.
Gaylord, B., Blanchette, C.A., Denny, M.W., 1994. Mechanical consequences of size in wave-swept algae. Ecol. Monogr. 64, 287–313.
Gaylord, B., Denny, M.W., Koehl, M.A.R., 2008. Flow forces on seaweeds: field evidence for roles of wave impingement and organism inertia. Biol. Bull. 215, 295–308.
Hay, C.H., 1990. The distribution of Macrocystis (Phaeophyta: Laminariales) as a biological indicator of cool sea surface temperature, with special reference to New Zealand waters. J. R. Soc. N.Z. 20, 313–336.
Hill, N.A., Pepper, A.R., Puotinen, M.L., Hughes, M.G., Edgar, G.J., Barrett, N.S., Stuart-Smith, R.D., Leaper, R., 2010. Quantifying wave exposure in shallow temperate reef systems: applicability of fetch models for predicting algal biodiversity. Mar. Ecol. Prog. Ser. 417, 83–95.
Huang, Z., McArthur, M., Radke, L., Anderson, T., Nichol, S., Siwabessy, J., Brooke, B., 2012. Developing physical surrogates for benthic biodiversity using co-located samples and regression tree models: a conceptual synthesis for a sandy temperate embayment. Int. J. Geogr. Inf. Sci. 26, 2141–2160.
Kain, J.M., 1982. Morphology and growth of the giant kelp *Macrocystis pyrifera* in New Zealand and California. Mar. Biol. 67, 143–157.
Kearney, M., Porter, W., 2009. Mechanistic niche modelling: combining physiological and spatial data to predict species' ranges. Ecol. Lett. 12, 334–350.
Leigh, E.G., Paine, R.T., Quinn, J.F., Suchanek, T.H., 1987. Wave energy and intertidal productivity. Proc. Natl. Acad. Sci. U.S.A. 84, 1314–1318.
Mach, K.J., Hale, B.J., Denny, M.W., Nelson, D.V., 2007. Death by small forces: a fracture and fatigue analysis of wave-swept macroalgae. J. Exp. Biol. 210, 2231–2243.
Mach, K.J., Tepler, S.K., Staaf, A.V., Bohnhoff, J.C., Denny, M.W., 2011. Failure by fatigue in the field: a model of fatigue breakage for the macroalga Mazzaella, with validation. J. Exp. Biol. 214, 1571–1585.
Madin, J.S., Connolly, S.R., 2006. Ecological consequences of major hydrodynamic disturbances on coral reefs. Nature 444, 477–480.
Nelson, W., 2008. Macroalgae of the Wellington south coast, Chapter 11. In: Gardner, J.P.A., Bell, J.J. (Eds.), The Taputeranga Marine Reserve. First Edition Publishers, Wellington, New Zealand.
NIWA, 2012. CliFlo. In: NIWA's National Climate Database on the Web, ⟨http://cliflo.niwa.co.nz⟩ (retrieved 25 July 2012).
Nyman, M.A., Brown, M.T., Neushul, M., Harger, B.W.W., Keogh, J.A., 1993. Mass distribution in the fronds of *Macrocystis pyrifera* from New Zealand and California. Hydrobiologia 260/261, 57–65.
Pande, A., Gardner, J.P.A., 2009. A baseline biological survey of the proposed Taputeranga Marine Reserve (Wellington, New Zealand): spatial and temporal variability along a natural environmental gradient. Aquat. Conserv. 19, 237–248.
Pickrill, R.A., Mitchell, J.S., 1979. Ocean wave characteristics around New Zealand. N.Z. J. Mar. Freshwater 13, 501–520.
R Core Team, 2013. R: A language and environment for statistical computing. In: R Foundation for Statistical Computing. R Core Team, Vienna, Austria, 3-900051-07-0 ⟨http://www.R-project.org/⟩.
Ris, R.C., Holthuijsen, L.H., Booij, N., 1999. A third-generation wave model for coastal regions: 2. Verification. J. Geophys. Res. 104, 7667–7681.
Romme, W.H., Everham, E.H., Frelich, L.E., Moritz, M.A., Sparks, R.E., 1998. Are large, infrequent disturbances qualitatively different from small, frequent disturbances? Ecosystems 1, 524–534.
Schiel, D.R., 1990. Macroalgal assemblages in New Zealand: structure, interactions and demography. Hydrobiologia 192, 59–76.
Seymour, R.J., Tegner, M.J., Dayton, P.K., Parnell, P.E., 1989. Storm wave induced mortality of giant kelp, *Macrocystis pyrifera*, in Southern California. Estuarine Coastal Shelf Sci. 28, 277–292.
Stewart, H.L., Fram, J.P., Reed, D.C., Williams, S.L., Brzezinski, M.A., MacIntyre, S., Gaylord, B., 2009. Differences in growth, morphology and tissue carbon and nitrogen of *Macrocystis pyrifera* within and at the outer edge of a giant kelp forest in California, USA. Mar. Ecol. Prog. Ser. 375, 101–112.
Thomsen, M.S., Wernberg, T., Kendrick, G.A., 2004. The effect of thallus size, life stage, aggregation and substratum conditions on the forces required to break or dislodge the small kelp *Ecklonia radiata*. Bot. Mar. 47, 454–460.
Tolman, H.L., 1997. User manual and system documentation of WAVEWATCH-III version 1.15. In: NOAA/NWS/NCEP/OMB Technical Note 151, 97 pp.
Toohey, B.D., Kendrick, G.A., Wernberg, T., Phillips, J.C., Malkin, S., Prine, J., 2004. The effects of light and thallus scour from *Ecklonia radiata* canopy on an associated foliose algal assemblage: the importance of photoacclimation. Mar. Biol. 144, 1019–1027.
Toohey, B.D., Kendrick, G.A., Harvey, E.S., 2007. Disturbance and reef topography maintain high local diversity in *Ecklonia radiata* kelp forests. Oikos 116, 1618–1630.
Utter, B.D., Denny, M.W., 1996. Wave-induced forces on the giant kelp *Macrocystis pyrifera* (Agardh): field test of a computational model. J. Exp. Biol. 199, 2645–2654.

Warner, J.C., Sherwood, C.R., Signell, R.P., Harris, C.K., Arango, H.G., 2008. Development of a three-dimension, regional, coupled wave, current, and sediment-transport model. Comput. Geosci. 34, 1284–1306.

Wernberg, T., Coleman, M., Fairhead, A., Miller, S., Thomsen, M., 2003. Morphology of *Ecklonia radiata* (Phaeophyta: Laminarales) along its geographic distribution in south-western Australia and Australasia. Mar. Biol. 143, 47–55.

Wright, L.D., 1976. Nearshore wave-power dissipation and the coastal energy regime of the Sydney-Jervis Bay region, New South Wales: a comparison. Mar. Freshwater Res. 27, 633–640.

Zimmerman, R.C., Kremer, J.N., 1986. In situ growth and chemical composition of the giant kelp, *Macrocystis pyrifera*: response to temporal changes in ambient nutrient availability. Mar. Ecol. Prog. Ser. 27, 277–285.